An Analytical Model for the Effects of the Spatial Resolution of Electrode Systems on the Spectrum of Cardiac Signals

Ferney Beltrán-Molina, Jesús Requena-Carrión, Felipe Alonso-Atienza, Nejib Zemzemi

An Analytical Model for the Effects of the Spatial Resolution of Electrode Systems on the Spectrum of Cardiac Signals

Ferney Beltrán-Molina, *Member, IEEE,* Jesús Requena-Carrión, *Member, IEEE,*
Felipe Alonso-Atienza, *Member, IEEE,* Nejib Zemzemi

***Abstract*—It has been suggested that the spatiotemporal characteristics of complex cardiac arrhythmias can be extracted from the spectrum of cardiac signals. However, the analysis of simple bioelectric models indicates that the spectrum of cardiac signals can be affected by the spatial resolution of the electrode system. In this study, we derive exact measurement transfer functions relating the spectrum of cardiac signals to the spatiotemporal dynamics of cardiac sources and estimate their bandwidths. The analysis of the measurement transfer bandwidths for dynamics with different degrees of spatiotemporal correlation shows that as the spatial resolution decreases, the bandwidth of the measurement transfer function decreases until it reaches a constant value. Moreover, this transition from decreasing to constant values is determined by the degree of spatiotemporal correlation of the underlying cardiac source. Motivated by our analytical results, we investigate in a realistic computer simulation environment the impact of additive noise on the accuracy of body-surface dominant frequency (DF) maps. Our simulation results show that meaningful DF values are obtained on those locations where the analytical measurement transfer bandwidth is wide. These findings suggest that the accuracy of body-surface DF maps can be limited by the low spatial resolution of body-surface electrode systems.**

***Index Terms*—Cardiac arrhythmias, dominant frequency, bioelectric model, spatiotemporal dynamics, spatial resolution.**

I. Introduction

Spectral analysis plays a prominent role in clinical and experimental electrophysiology. In cardiac electrophysiology, spectral techniques have been used to study complex arrhythmias, such as atrial fibrillation (AF) [1], [2], [3], [4], [5], [6], [7], [8], [9] and ventricular fibrillation (VF) [10], [11], [12], [13], [14], [15]. A notable example of the application of spectral analysis in cardiac electrophysiology is the technique known as dominant frequency (DF) mapping, which provides an estimation of the local activation rate of the myocardium. The analysis of DF maps of human fibrillating atria has allowed to identify anatomically localized, high-frequency sites [3], [5], [8]. These high-frequency sites have been hypothesized to be responsible for driving AF and hence, they have been proposed as potential targets for clinical ablation. In addition to the DF, other spectral features such as the peak frequency and the centroid frequency have been analyzed for different purposes, for instance for predicting the outcome of defibrillation [10], [11], [12] and for detecting VF [16], [17], [18].

When developing spectral techniques for analyzing cardiac arrhythmias, it is of importance to have a clear understanding of the nature of the spectrum of cardiac signals. A relevant consideration is how the choice of the electrode system can affect the spectrum of cardiac signals. In clinical and experimental cardiac electrophysiology, there exist a variety of electrode systems with different measurement characteristics. Existing electrode systems can be categorized as contact, intracardiac; non-contact, intracardiac; and body-surface electrode systems. Contact, intracardiac electrodes are positioned against the endocardium and measure the electrical activity of the heart locally. Non-contact, intracardiac electrodes also provide an endocardial view of the electrical activity of the heart, but they are not positioned directly against the endocardium. Finally, body-surface electrode systems provide a distant view of the electrical activity of the heart. With such a diversity of electrode systems, the question arises how spectra from different electrode systems relate to each other and to the underlying cardiac dynamics. In [19], the relationship between the spectrum of cardiac signals and the spatial resolution of electrode systems was investigated. This study showed that during cardiac dynamics with a high degree of spatiotemporal correlation, low spatial resolutions lead to low-pass type spectra. Similar conclusions have also been reached by applying Fourier spatiotemporal analysis to neurophysiology signals [20], [21]. Since electrode systems in close proximity to a bioelectric source have in general a higher spatial resolution than distant ones, it can be concluded that spectra from intracardiac and body-surface electrode systems reveal different aspects of the same underlying cardiac dynamics. Accordingly, when developing spectral techniques for investigating cardiac arrhythmias, it is of importance to consider possible filtering effects attributable to the measurement characteristics of the electrode systems.

Most theoretical studies investigating the nature of the spectrum of bioelectric signals, such as [19], [20], [21], have focused on simple, idealized models of the volume conductor, the electrode system and the spatiotemporal dynamics of the bioelectric source. Even though their results can explain spectral features observed experimentally, it is not well understood how they can extrapolate to more complex scenarios. By using

F. Beltrán-Molina is with the Universidad ECCI, Bogotá 111311, Colombia.
J. Requena-Carrión is with Queen Mary University of London, London E1 4NS, United Kingdom.
F. Alonso-Atienza is with University Rey Juan Carlos, Fuenlabrada 28943, Spain.
N. Zemzemi is with INRIA Bordeaux Sud-Ouest, 33405 Talence, France.

computer simulations, it has been shown that the degree of spatiotemporal correlation of complex cardiac dynamics, which quantifies their degree of spatiotemporal organization, plays an important role in determining the extent of filtering attributable to measuring [22], [23]. Observations such as these cannot be accounted for by current theoretical models and hence, they call for a generalized approach to investigate the spectrum of cardiac signals. Here, we develop an analytical approach that considers arbitrary volume conductors, arbitrary electrode systems and cardiac dynamics with an arbitrary degree of spatiotemporal correlation. We analytically derive measurement transfer functions relating the spectrum of cardiac signals to the spatiotemporal dynamics of cardiac sources and based on them, we obtain an approximation of their measurement transfer bandwidths. The measurement transfer bandwidth is a single parameter that allows us to quantitatively analyze, for each type of spatiotemporal dynamics, the spectral effects of the spatial resolution of the electrode system. We explore our analytical results in a realistic simulation environment, which we use to synthesize body-surface frequency maps induced by ventricular rhythms with different stimulation rates.

II. Bioelectric model

Following the approach presented in [19], we firstly derive an analytical model for the spectrum of cardiac signals. We model cardiac sources as a dipole field $\mathbf{J}(v,t) = [J_x(v,t), J_y(v,t), J_z(v,t)]^T$ within a volume V, where v is a location in V and t denotes time. A cardiac signal $s(t)$ induced by the dipole field $\mathbf{J}(v,t)$ is expressed as

$$s(t) = \int_V \mathbf{L}^T(v)\mathbf{J}(v,t)dv, \tag{1}$$

where $\mathbf{L}(v) = [L_x(v), L_y(v), L_z(v)]^T$ is the sensitivity distribution of the electrode system. The sensitivity distribution $\mathbf{L}(v)$ describes the ability of the electrode system to measure a single dipole located at v and is determined by the characteristics of both the volume conductor and the electrode system.

For a given frequency f, let $\sigma_{ab}(v,w,f)$ denote the cross-spectrum between two dipole components $J_a(v,t)$ and $J_b(w,t)$, where $a,b \in \{x,y,z\}$ and $v,w \in V$. The power spectrum $S(f)$ of cardiac signal $s(t)$ can be decomposed into nine cross-spectrum components $S_{ab}(f)$,

$$S(f) = \sum_{a,b\in\{x,y,z\}} S_{ab}(f), \tag{2}$$

which can be expressed as

$$S_{ab}(f) = \int_{V\times V} L_{ab}(v,w)\sigma_{ab}(v,w,f)dvdw. \tag{3}$$

In (3), we use the definition $L_{ab}(v,w) = L_a(v)L_b(w)$. Given a dipole location $v_0 \in V$, $\sigma_{ab}(v_0,v_0,f)$ describes the local dynamics of the cardiac source at v_0. Hence we will refer to $\sigma_{ab}(v,v,f)$ as the source *local spectrum*. By contrast, $S_{ab}(f)$ describes the dynamics of the cardiac source globally, at a spatial scale that is determined by $L_{ab}(v,w)$. Accordingly, we will refer to $S_{ab}(f)$ as the *global spectrum*.

III. Spectral effects of the spatial resolution

In this section, we analyze the effects of the spatial resolution of electrode systems on the spectrum of cardiac signals. We consider fully-uncorrelated sources, fully-correlated sources and partially-correlated sources. The definitions of fully-uncorrelated and fully-correlated sources follow the definitions presented in [19] and can be used to model, respectively, highly disorganized cardiac arrhythmias, such as some types of fibrillation, and highly regular rhythms, such as sinus rhythm. Partially-correlated cardiac sources are newly defined here and can be used to model complex arrhythmias with some degree of spatiotemporal organization.

In all of the cases, cardiac sources are assumed to have a uniform local spectrum, so that $\sigma_{ab}(v,v,f) = \sigma_{ab}(f)$. For each family of spatiotemporal dynamics, we first derive the measurement transfer function $H(f)$ relating the local spectrum to the global spectrum, $S_{ab}(f) = H(f)\sigma_{ab}(f)$. In this study, no assumptions on the electrode system and the volume conductor are made when deriving the measurement transfer functions. By lifting the restrictions on the type of electrode system and volume conductor, we greatly generalize previous studies [19], [20], [21]. In addition, we consider partially-correlated cardiac sources, which to the best of our knowledge have not been previously investigated.

Based on the measurement transfer function, we obtain an estimation of the measurement transfer bandwidth. In the derivation of the measurement transfer bandwidth, we consider an electrode system that measures the source activity within a compact volume $V_M \subset V$. We refer to V_M as the *resolution volume* and use it to characterize the spatial resolution of the electrode system. By denoting the sizes of V_M and V by respectively $|V_M|$ and $|V|$, we will say that the spatial resolution is high whenever $|V_M| \ll |V|$, whereas it is low whenever $|V_M| \simeq |V|$.

A. Fully-uncorrelated sources

In a fully-uncorrelated source with uniform local spectrum, the cross-spectrum between two dipole components is defined as

$$\sigma_{ab}(v,w,f) = \sigma_{ab}(f)\delta(v-w), \tag{4}$$

where $\delta(\cdot)$ is the delta function. By substituting (4) into (3), we can identify the measurement transfer function $H_{FU}(f)$:

$$H_{FU}(f) = \int_V L_{ab}(v,v)dv. \tag{5}$$

Equation (5) shows that the measurement transfer function $H_{FU}(f)$ is constant over the frequency domain. Hence, the measurement transfer bandwidth BW_{FU} is

$$BW_{FU} = \infty. \tag{6}$$

B. Fully-correlated sources

In a fully-correlated source, the activity of one dipole can be expressed as a delayed version of the activity of any other dipole. Let $\tau(v,w)$ denote the time-delay between the

activities of dipoles at locations v and w. The cross-spectrum between dipole components can be expressed as

$$\sigma_{ab}(v,w,f) = \sigma_{ab}(f)\exp\left[-j2\pi f\tau(v,w)\right]. \quad (7)$$

Based on $\tau(v,w)$, we define $g(\tau)$ as the density function of time-delays within V. In other words, the density function $g(\tau)$ quantifies the frequency that a pair of dipoles with time-delay τ is observed within V. By substituting (7) into (3), the following expression for the measurement transfer function $H_{FC}(f)$ can be identified (see Appendix):

$$H_{FC}(f) = H_g(f) * H_L(f), \quad (8)$$

where $*$ denotes convolution, $H_g(f)$ is the Fourier transform of $g(\tau)$ and $H_L(f)$ is a function of $L_{ab}(v,w)$ and $\tau(v,w)$. By assuming that the sensitivity distribution of the electrode system is concentrated on the resolution volume V_M, the measurement transfer bandwidth BW_{FC} can be approximated by

$$BW_{FC} \simeq k_M/d_M, \quad (9)$$

where d_M is the average distance between two dipoles in V_M and k_M is a proportionality constant.

C. Partially-correlated sources

We define the cross-spectrum between two dipole components in a partially-correlated source as

$$\begin{aligned}\sigma_{ab}(v,w,f) &= \sigma_{ab}(f)\exp\left[-j2\pi f\tau(v,w)\right] \\ &\times\ h_C\left[\tau(v,w)\right],\end{aligned} \quad (10)$$

where $h_C\left[\tau(v,w)\right]$ is the cross-spectrum decay and determines the correlation length d_C from which the correlation volume V_C can be obtained. By substituting (10) into (3), the measurement transfer function $H_{PC}(f)$ can be expressed as (see Appendix)

$$H_{PC}(f) = H_C(f) * H_g(f) * H_L(f), \quad (11)$$

where $H_C(f)$ is the Fourier transform of $h_C(\tau)$. If we assume that the sensitivity distribution is concentrated on the resolution volume V_M, the measurement transfer bandwidth BW_{PC} can be approximated by

$$BW_{PC} \simeq K_M/d_M + K_C/d_C. \quad (12)$$

where K_C is a proportionality constant. Equation (12) predicts that the measurement transfer bandwidth decreases with increasing resolution volumes until it reaches a saturation point, beyond which it remains constant. This behaviour depends on the size of the resolution volume, $|V_M|$, relative to the size of the correlation volume, $|V_C|$. Given a source with a correlation volume of size $|V_C|$ and a correlation length d_C, if $|V_M| \ll |V_C|$, then $d_M \ll d_C$ and $BW_{PC} \simeq K_M/d_M$. By contrast, when $|V_M| \gg |V_C|$, then $d_M \gg d_C$ and $BW_{PC} \simeq K_C/d_C$, i.e. the transfer bandwidth saturates and remains constant irrespective of $|V_M|$. Hence, from a measurement perspective, a partially-correlated source would appear correlated for $|V_M| \ll |V_C|$ and uncorrelated for $|V_M| \gg |V_C|$.

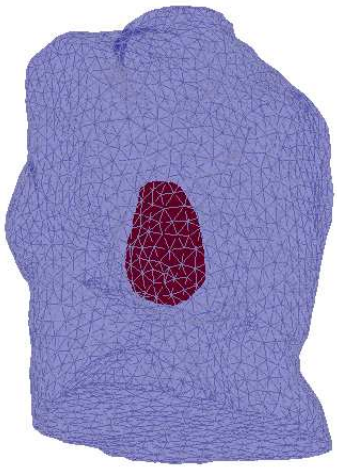

Fig. 1. Realistic geometry of the heart and torso used in our simulations.

Given a source characterized by a correlation length d_C, the relationship

$$d_M = d_C\frac{K_M}{K_C} \quad (13)$$

can be used to approximately identify in a simple way the spatial resolution beyond which the measurement transfer bandwidth BW_{PC} saturates.

IV. Computer simulations

We used a realistic simulation environment to analyze the spectrum of cardiac signals measured by body-surface electrode systems. In our simulation environment, cardiac activity was simulated by using a detailed model for the cardiac action potential and cardiac propagation, which was incorporated into a 3D realistic anatomical model of the heart and the torso. The 3D realistic anatomical model was obtained from the segmentation and discretization of CT scan images of a 43 years old woman. The resulting geometry model (Figure 1) consisted of triangular meshes of 5842 and 5742 nodes for the heart and the torso domains, respectively. This computer simulation environment allowed us to obtain the potentials at the body surface from the cardiac transmembrane potentials.

A. Numerical model

1) Model of action potential: Cardiac electrical activity at the cell level was simulated by using the ten Tusscher model of the action potential of human ventricular cells [24]. The temporal dynamics of the transmembrane potential v are described by the differential equation

$$\frac{dv}{dt} = f(v,t) = \frac{1}{C_m}(I_{ion}(v,t) + I_{st}(t)), \quad (14)$$

where t denotes time, I_{ion} is sum over all ionic currents defined in the ten Tusscher model, I_{st} is the external stimulation current, and C_m is the membrane capacity.

2) Model of cardiac tissue: Cardiac tissue behaves as a functional syncytium at the macroscopic level. We model cardiac tissue as an excitable medium $\Omega_H \in \mathbb{R}^3$ in which the propagation of the membrane potential $v = v(\mathbf{r}_H, t)$, with $\mathbf{r}_H \in \Omega_H$, is mathematically described according to the so-called monodomain formalism, which is formulated as the following reaction-diffusion equation

$$\frac{\partial v}{\partial t} = \nabla D \cdot (\nabla v) + f(v,t) \quad \text{in } \Omega_H, \tag{15}$$

with the no-flux boundary condition

$$\frac{\partial v}{\partial \mathbf{n}} = 0 \quad \text{on } \partial\Omega_H, \tag{16}$$

where D is the harmonic mean of the intracellular and the extracellular conductivity tensors, D_i and D_e,

$$D = D_i(D_i + D_e)^{-1} D_e,$$

$\partial\Omega_H$ is the boundary of Ω_H and $\mathbf{n}$ denotes its normal. The initial conditions for v and the model state variables were obtained at the recovery phase of the transmembrane potential after stimulating the tissue during 10 min at 1 Hz and the value of the conductivity tensor D was set to obtain a conduction velocity of approximately $50\,\mathrm{cm/s}$.

3) Model of voltage recordings at the body surface: According to the Volume Conductor Theory [25], the electric potential registered by an electrode placed at $\mathbf{r_T}$ within the torso surface Ω_T is given by

$$\varphi(\mathbf{r}_T, t) = \frac{1}{4\pi c_0} \int_{\Omega_H} \frac{\nabla D \cdot (\nabla v(\mathbf{r}_H, t))}{R(\mathbf{r}_H, \mathbf{r}_T)}\, d\Omega_H \tag{17}$$

where $R(\mathbf{r}_H, \mathbf{r}_T) = ||\mathbf{r}_T - \mathbf{r}_H||$ is the distance from the source location point $\mathbf{r}_H$ to the observation point $\mathbf{r}_T$, c_0 is the medium conductivity (assumed homogeneous and set to $1\,\mathrm{S/m}$), and $v(\mathbf{r}_H, t)$ is the solution of (15). Using a finite element approach, equation (17) can be extended to an arbitrary number of recording sites as

$$\boldsymbol{\varphi}(t) = \mathbf{A} \cdot \mathbf{v}(t) \tag{18}$$

where $\mathbf{A}$ is the so-called transfer matrix that linearly relates the transmembrane potential distribution at the heart elements $\mathbf{v}(t)$ to the body-surface potentials at the torso elements $\boldsymbol{\varphi}(t)$.

B. Analysis of body-surface spectra

In our simulation environment, we generated three uniform spatiotemporal dynamics by stimulating the ventricular apex at, respectively, 1 Hz, 2 Hz and 3 Hz. As shown in Figure 2, the generated dynamics consisted of plane wavefronts emanating from the ventricular apex with a frequency equal to the stimulation rate. By using (18) we obtained the time-varying body-surface potential distribution $\boldsymbol{\varphi}(t)$ induced by the simulated transmembrane potential $\mathbf{v}(t)$. White gaussian noise was added to body-surface potentials to analyze the impact of noise on the estimation of the DF. We included in our analysis signal-to-noise ratios (SNR) ranging from 1 to 25 dB.

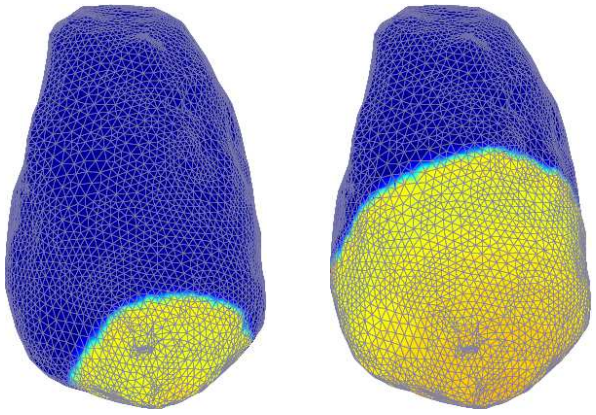

(a) (b)

Fig. 2. Wavefront generated by stimulating the ventricular apex (a) 10 ms and (b) 25 ms after the stimulation of the ventricular apex.

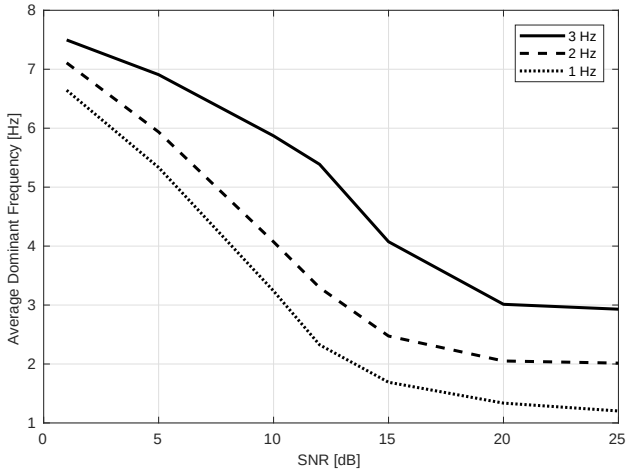

Fig. 3. Impact of noise on the average body-surface DF value for each simulated stimulation rate.

Body-surface spectra were estimated by applying Welch's method to the noisy potentials induced at each torso location. Estimated spectra were used to obtain DF values as defined in [26]. The signal processing pipeline that defines the DF consists of three stages, namely band-pass filtering at 40 to 250 Hz, rectification and finally low-pass filtering with a 20-Hz cutoff. It is worth noting that rectification is a non-linear operation that produces new frequency components, some of which lie outside the passband defining the first filtering stage. In addition, we used our analytical results derived in Section III to estimate the measurement transfer bandwidth at each torso location.

C. Simulation results

The DF values obtained at the ventricles were uniform and consistent with the simulated stimulation rates, namely 1 Hz, 2 Hz and 3Hz. However, the DF values obtained from the body-surface potentials differed from the underlying stimulation rates in the presence of noise. Figure 3 shows for each stimulation rate the average DF value as a function of the SNR. For low SNR, the average DF value was biased towards

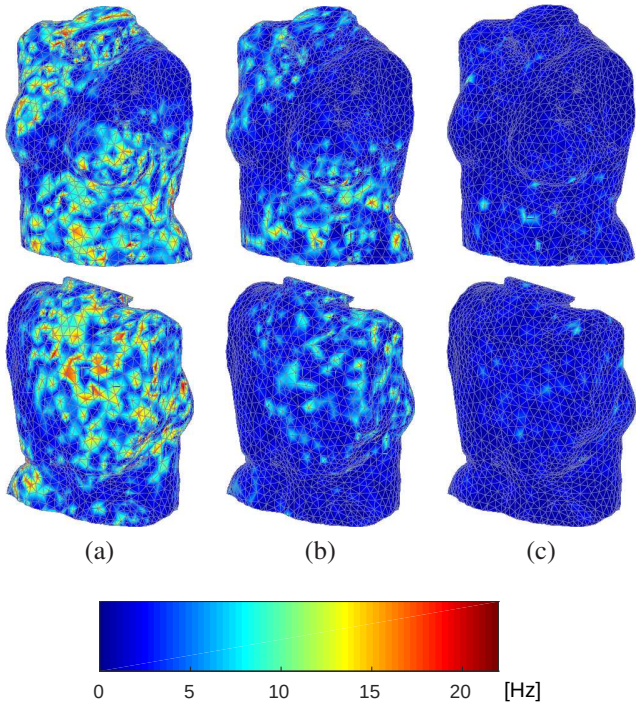

Fig. 4. DF values for a stimulation rate of 1 Hz and SNR of (a) 5 dB (b) 10 dB and (c) 15 dB.

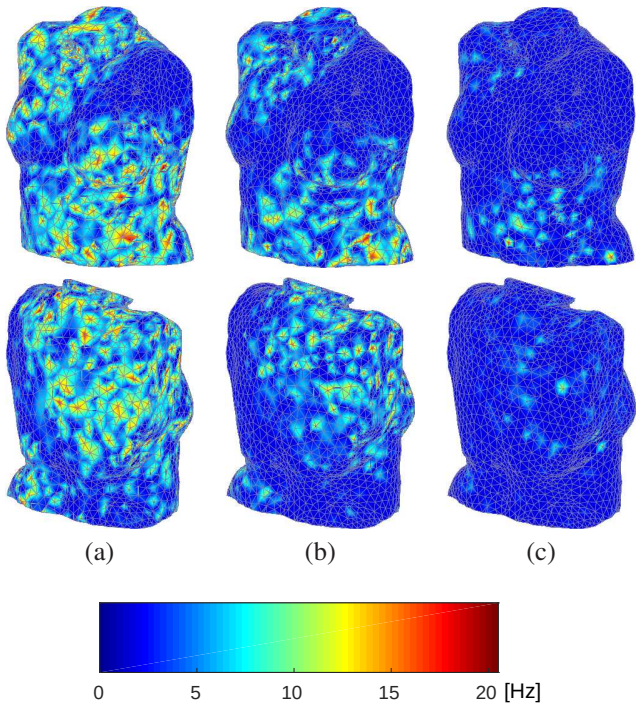

Fig. 5. DF values for a stimulation rate of 2 Hz and SNR of (a) 5 dB (b) 10 dB and (c) 15 dB.

higher values, whereas for higher SNR values, the average DF approached the underlying stimulation rates of 1 Hz, 2 Hz and 3 Hz, respectively. Therefore, our simulations suggest that the quality of the estimation of DF values can be affected by the presence of noise.

Figures 4, 5 and 6 show the body-surface DF maps corresponding to a stimulation rate of respectively 1 Hz, 2 Hz and 3Hz, for three increasing SNR values. These distributions of body-surface DF values are difficult to explain without a mathematical framework relating the spectrum of cardiac signals to the underlying cardiac spatiotemporal dynamics. In our simulations, the distribution of body-surface DF values in noisy scenarios revealed a clear pattern. Two regions could be identified in all cases. The first region was an approximately belt-shaped area surrounding the torso and connecting the left shoulder with the right ilium. Within this region, DF values were uniform and numerically close to the underlying stimulation rate. The actual shape and width of this region was different for different SNR values. Specifically, we observed that the higher the SNR the wider the belt. However, for low SNR values, this region was restricted to the left shoulder. The area of the torso outside this belt-shaped region constituted the second region and within it, DF values appeared to be randomly distributed. Because of the dependence of the width of the belt on the SNR, higher SNR values led to more uniform body-surface DF values that were consistent with the underlying stimulation rate.

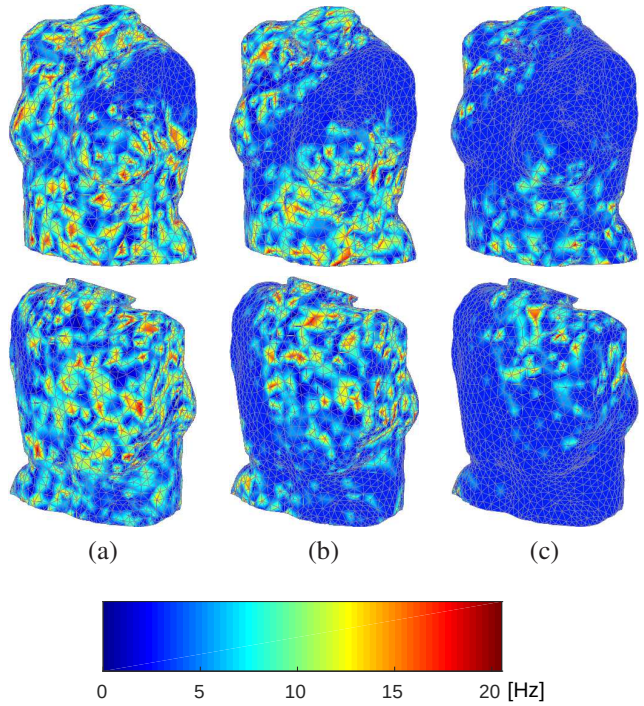

Fig. 6. DF values for a stimulation rate of 3 Hz and SNR of (a) 5 dB (b) 10 dB and (c) 15 dB.

Our mathematical formalism allowed us to explain the body-surface DF maps shown in Figures 4, 5 and 6. According to our formalism, the spectrum of body-surface signals can be expressed as a low-pass filtered version of the spectrum at the tissue level. Figure 7 shows the measurement transfer bandwidths at each site of the torso for a stimulation rate of 2 Hz. Similar distributions for the measurement transfer bandwidth were obtained for stimulation rates of 1 Hz and 3 Hz. Figure 7 shows that the measurement transfer bandwidth values were not uniform over the torso, with some regions suffering more

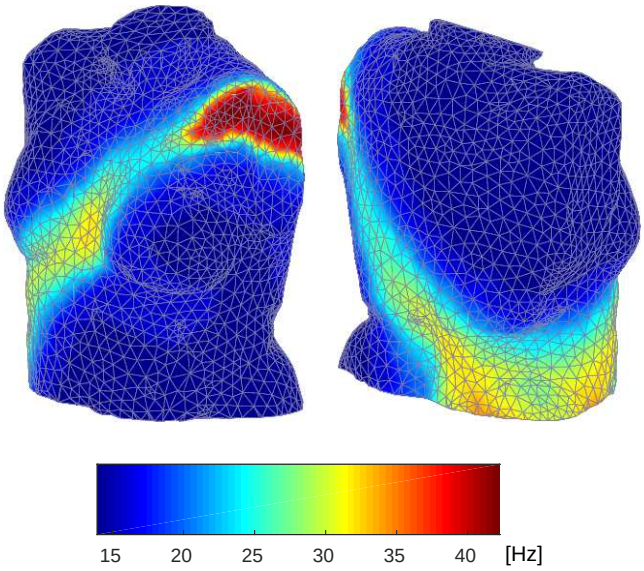

Fig. 7. Measurement transfer bandwidth analytically obtained for a stimulation rate of 2 Hz.

aggressive low-pass filtering effects than others. Specifically, the region around the left shoulder presents bandwidth values reaching 40 Hz and a belt connecting left shoulder to right ilium with high bandwidth values is clearly visible. This non-uniform distribution of bandwidth values resembles the distribution of DF values shown in Figures 4, 5 and 6 and indeed explains them. Since the signal processing technique defining the DF uses a first stage of band-pass filtering, the ability to extract physiologically meaningful DF values was more compromised in sites with a low measurement transfer bandwidth. Therefore, in a noisy environment only those areas were the measurement transfer bandwidth was high provided meaningful DF values. Therefore, for a given SNR value, a bandwidth threshold value can be defined only above which meaningful DF values can be obtained. This bandwidth threshold decreases as the SNR increases, producing the widening of the belt containing meaningful DF values, in other words, extending the region within which meaningful DF values can be found.

V. Discussion and conclusion

The heart is a bioelectric organ formed by coupled, excitable cells that collectively give rise to spatiotemporal dynamics. The spatiotemporal characteristics of cardiac dynamics can be related to the function of the heart and, because of their bioelectric nature, they can also manifest in signals measured by electrode systems. This results in a relationship between cardiac function and signal features, which forms the basis of the analysis of cardiac signals. However, although this relationship can be straightforward for simple, regular spatiotemporal dynamics such as the heart during sinus rhythm, it can be very intricate for complex ones such as cardiac fibrillation.

Signal processing techniques based on spectral analysis have been developed in cardiac electrophysiology to study complex arrhythmias. One of the main applications of spectral analysis is the characterization of the spatiotemporal dynamics of AF. By obtaining DF maps of the fibrillating atria [3], [5], [8], anatomically localized, high-frequency sites have been identified, which supports the idea of the existence of AF drivers. Other spectral features such as the organization index (OI) [1] and the multivariate organization index (MOI) [6] have also been proposed to quantify the degree of spatiotemporal organization of AF.

The increasing interest in applying spectral techniques to analyze complex arrhythmias has come hand-in-hand with the need to improve our understanding of the nature of cardiac spectrum. Some authors have contributed to clarifying the meaning of cardiac spectrum from a signal processing perspective [27], [28]. In [19] a measurement perspective was adopted and a mathematical formalism was developed for investigating the bioelectric nature of cardiac spectrum. This formalism allowed to express the spectrum of cardiac signals in terms of the spatiotemporal dynamics of cardiac sources and the sensitivity distribution of the electrode system. By analyzing this connection, it was shown that when the underlying dynamics are fully correlated, low spatial resolutions lead to low-pass type cardiac spectra. The main take-home message of [19] was that the effects of measuring needs to be taken into consideration when analyzing the spectrum of cardiac signals.

Here, we have generalized those previous analytical results by considering arbitrary volume conductors and electrode systems, and cardiac sources with arbitrary degrees of spatiotemporal correlation. We have analytically derived measurement transfer functions and bandwidths relating the spectrum of cardiac signals to the spatiotemporal dynamics of cardiac sources. Our analysis shows that the measurement transfer bandwidth can be expressed in terms of the degree of spatiotemporal correlation of the cardiac source and the spatial resolution of the electrode system. This relationship has allowed us to make the following prediction about the effects of the spatial resolution on the spectrum of cardiac signals. By increasing the resolution volume, the bandwidth of the measured cardiac signal decreases until it reaches a point beyond which it saturates. Bandwidth saturation occurs whenever the resolution volume of the electrode system is larger than the correlation volume of the cardiac source.

We have illustrated in a simulation environment how DF maps can be distorted as a consequence of the filtering effects attributable to measuring. By simulating a regular, fast rhythm, we have synthesized cardiac transmembrane potentials and body-surface potentials. Our simulations show that the body-surface potentials can be expressed as a low-pass version of the transmembrane potentials and that the associated filter is in general different at each torso site. These results are accurately predicted by our formalism. The filtering attributable to measuring can in turn affect body-surface DF values. This distortion is more apparent in noisy environments, although in theory it could also happen in noise-free scenarios.

Our results indicate that, in general, spectral features of cardiac signals cannot be translated per se into specific features of the underlying spatiotemporal dynamics without careful consideration of the effects of the process of measurement. Measurands, in our case spectral features, are after all defined by the measuring process itself. Hence, the interpretation

of a spectral feature such as the peak frequency would in principle not be the same for intracardiac signals and for body-surface signals, since intracardiac and body-surface electrode systems define a different measuring process. In the context of DF mapping, different choices of electrode systems have been used to obtain cardiac signals. These include sequential, contact, intracardiac electrodes [2], [3], [4], [5], [8], non-contact, intracardiac electrode arrays [29], [9] and body-surface electrode arrays [30], [31], [32], [7], [33]. Based on our formalism, when using body-surface electrode systems we would expect to obtain distorted versions of the spectra provided by intracardiac systems, since their spatial resolution is lower. Therefore, the DF maps obtained by intracardiac mapping should be expected to be different from the DF maps obtained by body-surface mapping, even when the underlying arrhythmias are highly regular.

The measurement transfer functions and bandwidths obtained in this paper for uncorrelated, fully-correlated and partially-correlated cardiac rhythms, have been derived analytically from well-established bioelectric models. However, even though the derived measurement transfer functions are exact and not approximations, the extent of their impact on human cardiac spectra would need to be further assessed. Realistic computer simulation environments such as the one used in this paper, provide an excellent framework for systematically exploring our mathematical formalism. Computer simulation approaches have been used in previous studies to investigate the spectra of cardiac rhythms with complex spatiotemporal dynamics [22], [23], and the analysis of their simulation results agree with our analytical claims, which relate the bandwidth of cardiac signals with the spatial resolution of the electrode system and the correlation volume of the underlying cardiac source. Further validations in clinical settings are nevertheless essential to assess the extent of the filtering effects attributable to measuring in real-world scenarios. In order to carry out a clinical assessment of our analytical predictions, intracardiac and body-surface recordings need to be simultaneously recorded during different types of arrhythmias, so that the relationship between local and global spectra i.e. the measurement transfer function, can be identified for each type of arrhythmia. Previous clinical studies have indeed recorded simultaneously intracradiac and body-surface signals to empirically investigate DF maps during AF [7], [34]. One of the main conclusions of these studies is that body-surface DF mapping is able to capture regional differences in atrial activation rates during AF. Interestingly, the results presented in [34] seem to indicate that there is a systematic difference between the body-surface and intracardiac DF values and that this difference presents a non-uniform distribution over the torso. These observations agree with our analytical results and might be explained by suitable measurement transfer functions.

A better understanding of the actual filtering effects of measuring can help in devising new signal processing techniques for analysing cardiac arrhythmias. One consequence of our prediction that the extent of filtering depends on the degree of spatiotemporal correlation of the underlying dynamics [c.f. (12)], is that in order to compensate for such filtering effects, a prior estimation of the degree of cardiac spatiotemporal correlation is needed. Current mapping approaches obtain DF values at each torso location by solely analyzing the signal recorded at the actual location. Interestingly, body-surface potentials can be jointly analyzed to produce an indirect estimation of the degree of spatiotemporal correlation. Consequently, based on our formalism we can conclude that improved DF estimations could be obtained by analyzing the signal at the location of interest jointly with signals from neighboring locations, as information about the underlying degree of spatiotemporal correlation would be potentially incorporated. Finally, even though our study focuses on cardiac arrhythmias, our analytical results could be applied to other bioelectric signals, such as encephalography (EEG) signals. Spectral analysis is one of the most important tools in EEG studies and it has been long recognized that EEG and cortical source activity will in general exhibit different spectra [21]. Our study provides a quantitative framework to also investigate the spectrum of EEG signals. Specifically, our main conclusion that the spatiotemporal characteristics of the underlying rhythm plays an important role in the final filtering produced by measuring, can be of importance in EEG studies. Interestingly, recently proposed methods for analyzing EEG signals leverage spatial relationships between EEG sites for frequency recognition. In [35] spatial filters are built from EEG training datasets to provide reference signals which are needed for frequency recognition in steady-state visual evoked potentials. Their results show that the proposed method improves frequency recognition, compared to conventional methods that do not use any spatial information. This supports the take-home message that by incorporating prior knowledge about the underlying degree of spatiotemporal correlation, spectral features can potentially be extracted with higher accuracy.

APPENDIX A
THE MEASUREMENT TRANSFER FUNCTION DURING FULLY- AND PARTIALLY-CORRELATED DYNAMICS

Let us start off by considering a bioelectric source with partially-correlated dynamics and uniform local spectrum. By substituting (10) into (3), its measurement transfer function $H_{PC}(f)$, can be expressed as

$$H_{PC}(f) = \int_{V\times V} L_{ab}(v,w)e^{-j2\pi f\tau(v,w)}h_C\left[\tau(v,w)\right]dvdw \tag{19}$$

Let us define $g(L_{ab},\tau)$ as the joint density function of the pairs of values $\{L_{ab}(v,w),\tau(v,w)\}$ for $v,w \in V$. By applying Bayes Theorem, the joint density function $g(L_{ab},\tau)$ can be expressed as

$$g(L_{ab},\tau) = g(L_{ab}|\tau)g(\tau) \tag{20}$$

where $g(L_{ab}|\tau)$ is the conditional density function of $L_{ab}(v,w)$ given $\tau(v,w)$, and $g(\tau)$ is the density function of $\tau(v,w)$.

By integrating with respect to L_{ab} and τ and using (20), (19) can be expressed as

$$H_{PC}(f) = \int_{-\infty}^{\infty} e^{-j2\pi f\tau}h_C(\tau)g(\tau)\int_{-\infty}^{\infty} L_{ab}g(L_{ab}|\tau)dL_{ab}d\tau. \tag{21}$$

The integral

$$\bar{L}_{ab}(\tau_0) = \int_{-\infty}^{\infty} L_{ab} g(L_{ab}|\tau_0) dL_{ab} \quad (22)$$

corresponds to the mean value of $L_{ab}(v,w)$ for all pairs of locations $\{v,w\}$ such that $\tau(v,w) = \tau_0$.

By using the definition (22) in (21) we finally obtain

$$\begin{aligned} H_{PC}(f) &= \int_{-\infty}^{\infty} e^{-j2\pi f\tau} h_C(\tau) g(\tau) \bar{L}_{ab}(\tau) d\tau \\ &= H_C(f) * H_g(f) * H_L(f) \end{aligned} \quad (23)$$

where $H_C(f)$, $H_g(f)$ and $H_L(f)$ are, respectively, the Fourier transforms of the functions $h_C(\tau)$, $g(\tau)$ and $\bar{L}_{ab}(\tau)$. By setting $h_C(\tau) = 1$, the measurement transfer function during fully-correlated dynamics, $H_{FC}(f)$, can be readily obtained.

Finally, the bandwidth of $H_C(f)$ is inversely related to the degree of spatiotemporal correlation at the source, which can be quantified by the correlation length d_C, whereas $H_\tau(f) * H_L(f)$ is inversely related to the scale of the measurement, which can be quantified by the length d_M. Hence, the bandwidth BW_{PC} of the measurement transfer function $H_{PC}(f)$ can be approximated by

$$BW_{PC} \simeq K_M/d_M + K_C/d_C, \quad (24)$$

where K_M and K_C are proportionality constants. Furthermore, if $d_C \to \infty$ ($d_C \to 0$) the source becomes fully-correlated (respectively, fully-uncorrelated). This is mirrored in the dependence of the measurement transfer bandwidth with d_C. If $d_C \to \infty$ ($d_C \to 0$), then $BW_{PC} \to K_M/d_M$ (respectively, $BW_{PC} \to \infty$).

REFERENCES

[1] T. H. Everett, L.-C. Kok, R. Vaughn, J. Moorman, and D. Haines, "Frequency domain algorithm for quantifying atrial fibrillation organization to increase defibrillation efficacy," *IEEE Transactions on Biomedical Engineering*, vol. 48, no. 9, pp. 969–978, 2001.

[2] S. Lazar, S. Dixit, F. E. Marchlinski, D. J. Callans, and E. P. Gerstenfeld, "Presence of left-to-right atrial frequency gradient in paroxysmal but not persistent atrial fibrillation in humans," *Circulation*, vol. 110, no. 20, pp. 3181–3186, 2004.

[3] P. Sanders, O. Berenfeld, M. Hocini, P. Jais, R. Vaidyanathan, L. F. Hsu, S. Garrigue, Y. Takahashi, M. Rotter, F. Sacher, C. Scavee, R. Ploutz-Snyder, J. Jalife, and M. Haissaguerre, "Spectral analysis identifies sites of high-frequency activity maintaining atrial fibrillation in humans," *Circulation*, vol. 112, no. 6, pp. 789–797, 2005.

[4] F. Atienza, J. Almendral, J. Moreno, R. Vaidyanathan, A. Talkachou, J. Kalifa, A. Arenal, J. P. Villacastin, E. G. Torrecilla, A. Sanchez, R. Ploutz-Snyder, J. Jalife, and O. Berenfeld, "Activation of inward rectifier potassium channels accelerates atrial fibrillation in humans: evidence for a reentrant mechanism," *Circulation*, vol. 114, no. 23, pp. 2434–2442, 2006.

[5] F. Atienza, J. Almendral, J. Jalife, S. Zlochiver, R. Ploutz-Snyder, E. G. Torrecilla, A. Arenal, J. Kalifa, F. Fernández-Avilés, and O. Berenfeld, "Real-time dominant frequency mapping and ablation of dominant frequency sites in atrial fibrillation with left-to-right frequency gradients predicts long-term maintenance of sinus rhythm," *Heart Rhythm*, vol. 6, no. 1, pp. 33 – 40, 2009.

[6] L. Uldry, J. Van Zaen, Y. Prudat, L. Kappenberger, and J.-M. Vesin, "Measures of spatiotemporal organization differentiate persistent from long-standing atrial fibrillation," *Europace*, vol. 14, no. 8, pp. 1125–1131, 2012.

[7] M. S. Guillem, A. M. Climent, J. Millet, Á. Arenal, F. Fernández-Avilés, J. Jalife, F. Atienza, and O. Berenfeld, "Noninvasive localization of maximal frequency sites of atrial fibrillation by body surface potential mapping," *Circulation: Arrhythmia and Electrophysiology*, vol. 6, no. 2, pp. 294–301, 2013.

[8] K. Kumagai, T. Sakamoto, K. Nakamura, S. Nishiuchi, M. Hayano, T. Hayashi, T. Sasaki, K. Aonuma, and S. Oshima, "Combined dominant frequency and complex fractionated atrial electrogram ablation after circumferential pulmonary vein isolation of atrial fibrillation," *Journal of Cardiovascular Electrophysiology*, vol. 24, no. 9, pp. 975–983, 2013.

[9] J. L. Salinet, J. H. Tuan, A. J. Sandilands, P. J. Stafford, F. S. Schlindwein, and G. A. Ng, "Distinctive patterns of dominant frequency trajectory behavior in drug-refractory persistent atrial fibrillation: Preliminary characterization of spatiotemporal instability," *Journal of Cardiovascular Electrophysiology*, vol. 25, no. 4, pp. 371–379, 2014.

[10] H. U. Strohmenger, K. H. Lindner, and C. G. Brown, "Analysis of the ventricular fibrillation ecg signal amplitude and frequency parameters as predictors of countershock success in humans," *Chest*, vol. 111, no. 3, pp. 584–589, Mar 1997.

[11] T. Eftestøl, K. Sunde, S. O. Aase, J. H. Husoy, and P. A. Steen, "Predicting outcome of defibrillation by spectral characterization and nonparametric classification of ventricular fibrillation in patients with out-of-hospital cardiac arrest," *Circulation*, vol. 102, no. 13, pp. 1523–1529, 2000.

[12] I. Jekova, F. Mougeolle, and A. Valance, "Defibrillation shock success estimation by a set of six parameters derived from the electrocardiogram," *Physiological Measurement*, vol. 25, no. 5, pp. 1179–1188, 2004.

[13] I. Panfilov, N. A. Lever, B. H. Smaill, and P. D. Larsen, "Ventricular fibrillation frequency from implanted cardioverter defibrillator devices," *Europace*, vol. 11, no. 8, pp. 1052–1056, 2009.

[14] M. E. Mollerus, C. Renier, and M. Lipinski, "Spectral methods to distinguish ventricular fibrillation from artefact in implantable cardioverter-defibrillators," *Europace*, vol. 13, no. 9, pp. 1346–1351, 2011.

[15] J. Requena-Carrión, F. Alonso-Atienza, E. Everss, J. J. Sánchez-Muñoz, M. Ortiz, A. García-Alberola, and J. Rojo-Álvarez, "Analysis of the robustness of spectral indices during ventricular fibrillation," *Biomedical Signal Processing and Control*, vol. 8, no. 6, pp. 733–739, 11 2013.

[16] S. Barro, R. Ruiz, D. Cabello, and J. Mira, "Algorithmic sequential decision-making in the frequency domain for life threatening ventricular arrhythmias and imitative artefacts: a diagnostic system," *Journal of Biomedical Engineering*, vol. 11, no. 4, pp. 320 – 328, 1989.

[17] U. Ayala, U. Irusta, J. Ruiz, T. Eftestøl, J. Kramer-Johansen, F. Alonso-Atienza, E. Alonso, and D. González-Otero, "A reliable method for rhythm analysis during cardiopulmonary resuscitation." *Biomed Res Int*, vol. 2014, p. 872470, 2014.

[18] F. Alonso-Atienza, E. Morgado, L. Fernandez-Martinez, A. Garcia-Alberola, and J. Rojo-Alvarez, "Detection of life-threatening arrhythmias using feature selection and support vector machines," *IEEE Transactions on Biomedical Engineering*, vol. 61, no. 3, pp. 832–840, 2014.

[19] J. Requena-Carrión, F. A. Beltrán-Molina, and A. G. Marques, "Relating the spectrum of cardiac signals to the spatiotemporal dynamics of cardiac sources," *Biomedical Signal Processing and Control*, vol. 8, no. 6, pp. 935–944, 2013.

[20] P. L. Nunez, *NeoCortical Dynamics and Human EEG Rhythm*, 1st ed. Oxford University Press, 1995.

[21] P. L. Nunez and R. Srinivasan, *Electric Fields of the Brain: The Neurophysics of EEG*, 2nd ed. Oxford University Press, 2006.

[22] F. A. Beltran-Molina, E. Cruz-Salazar, and J. Requena-Carrion, "Dependence of cardiac spectrum on the spatial resolution of the electrode systems in a realistic model of the canine ventricles," in *Engineering in Medicine and Biology Society (EMBC), 2015 37th Annual International Conference of the IEEE*, 2015, pp. 2223–2226.

[23] F. A. Beltran-Molina, L. C. Salgado, L. J. Martinez, and J. Requena-Carrion, "Analysis of the spectrum of cardiac signals during partially correlated spatiotemporal dynamics: A simulation approach," in *Computing in Cardiology (CinC)*. IEEE, 2015.

[24] K. H. W. J. ten Tusscher, D. Noble, P. J. Noble, and A. V. Panfilov, "A model for human ventricular tissue," *American Journal of Physiology - Heart and Circulatory Physiology*, vol. 286, no. 4, pp. H1573–H1589, 2004.

[25] J. Malmivuo and R. Plonsey, *Bioelectromagnetism: principles and applications of bioelectric and biomagnetic fields*. New York: Oxford University Press, 1995.

[26] G. W. Botteron and J. M. Smith, "Quantitative assessment of the spatial organization of atrial fibrillation in the intact human heart," *Circulation*, vol. 93, pp. 513–518, 1996.

[27] G. Fischer, M. C. Stuhlinger, C. N. Nowak, L. Wieser, B. Tilg, and F. Hintringer, "On computing dominant frequency from bipolar intracardiac electrograms," *IEEE Transactions on Biomedical Engineering*, vol. 54, no. 1, pp. 165–169, 2007.

[28] J. Ng and J. J. Goldberger, "Understanding and interpreting dominant frequency analysis of af electrograms," *Journal of Cardiovascular Electrophysiology*, vol. 18, no. 6, pp. 680–685, 2007.

[29] J. W. Jarman, T. Wong, P. Kojodjojo, H. Spohr, J. E. Davies, M. Roughton, D. P. Francis, P. Kanagaratnam, V. Markides, D. W. Davies, and N. S. Peters, "Spatiotemporal behavior of high dominant frequency during paroxysmal and persistent atrial fibrillation in the human left atriumclinical perspective," *Circulation: Arrhythmia and Electrophysiology*, vol. 5, no. 4, pp. 650–658, 2012.

[30] M. S. Guillem, A. M. Climent, F. Castells, D. Husser, J. Millet, A. Arya, C. Piorkowski, and A. Bollman, "Noninvasive mapping of human atrial fibrillation," *Journal of Cardiovascular Electrophysiology*, vol. 20, no. 5, pp. 507–513, 2009.

[31] P. S. Cuculich, Y. Wang, B. D. Lindsay, M. N. Faddis, R. B. Schuessler, R. J. Damiano, L. Li, and Y. Rudy, "Noninvasive characterization of epicardial activation in humans with diverse atrial fibrillation patterns," *Circulation*, vol. 122, no. 14, pp. 1364–1372, 2010.

[32] M. Haissaguerre, M. Hocini, A. J. Shah, N. Derval, F. Sacher, P. Jais, and R. Dubois, "Noninvasive panoramic mapping of human atrial fibrillation mechanisms: A feasibility report," *Journal of Cardiovascular Electrophysiology*, vol. 24, no. 6, pp. 711–717, 2013.

[33] M. Rodrigo, M. S. Guillem, A. M. Climent, J. Pedrón-Torrecilla, A. Liberos, J. Millet, F. Fernández-Avilés, F. Atienza, and O. Berenfeld, "Body surface localization of left and right atrial high-frequency rotors in atrial fibrillation patients: A clinical-computational study," *Heart Rhythm*, vol. 11, no. 9, pp. 1584–1591, 2014.

[34] M. Rodrigo, A. Climent, A. Liberos, F. Fernández-Aviles, F. Atienza, M. Guillem, and O. Berenfeld, "Minimal configuration of body surface potential mapping for discrimination of left versus right dominant frequencies during atrial fibrillation," *Pacing and Clinical Electrophysiology*, 2017. [Online]. Available: http://dx.doi.org/10.1111/pace.13133

[35] Y. Zhang, G. Zhou, J. Jin, X. Wang, and A. Cichocki, "Frequency recognition in ssvep-based bci using multiset canonical correlation analysis," *International Journal of Neural Systems*, vol. 24, no. 04, p. 1450013, 2014.